




# Beta inputs to motor neurons do not directly contribute to volitional force modulation

Blanka Zicher<sup>1</sup> , Jaime Ibáñez<sup>1,2,3</sup>  and Dario Farina<sup>1</sup> 

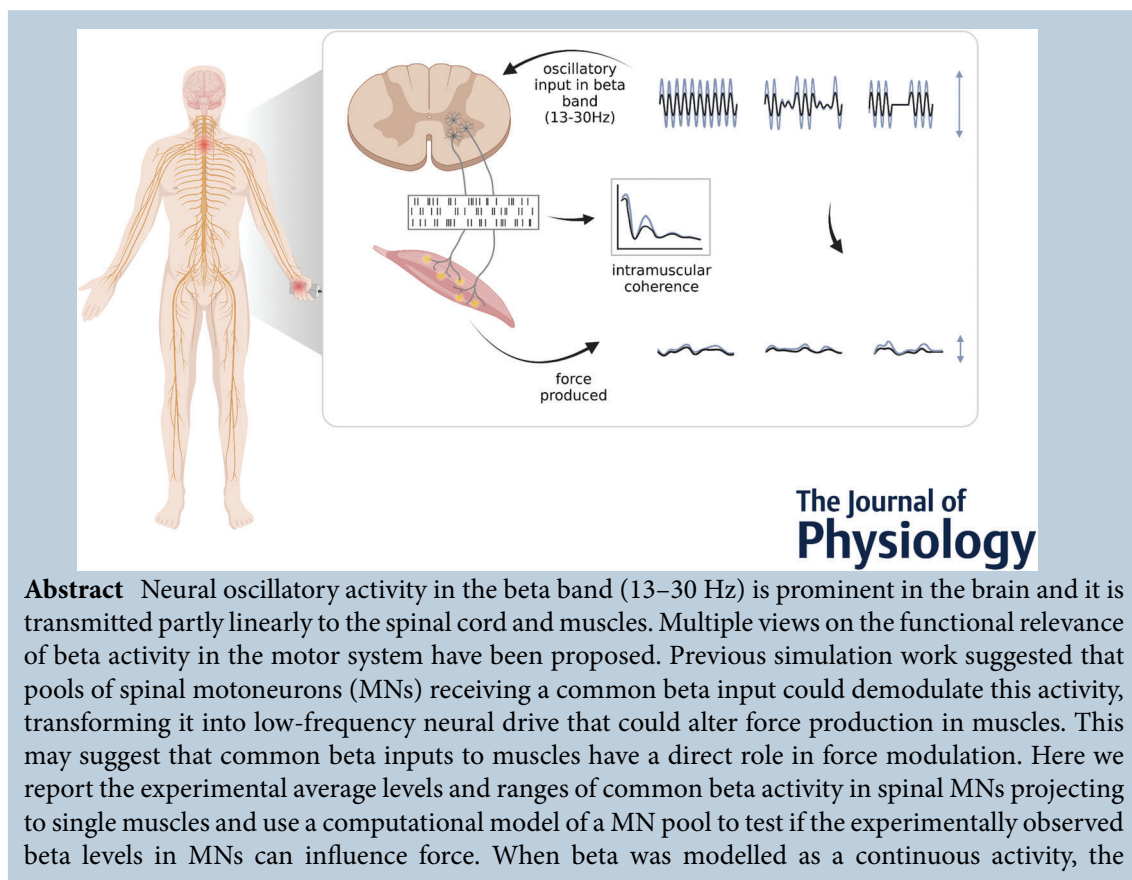
<sup>1</sup>Department of Bioengineering, Imperial College, London, UK

<sup>2</sup>BSICoS, IIS Aragón, Universidad de Zaragoza, Zaragoza, Spain

<sup>3</sup>Department for Clinical and Movement Neurosciences, Institute of Neurology, University College London, London, UK

Handling Editors: Richard Carson & Mathew Piasecki

The peer review history is available in the Supporting Information section of this article (<https://doi.org/10.1113/JP283398#support-information-section>).



**Abstract** Neural oscillatory activity in the beta band (13–30 Hz) is prominent in the brain and it is transmitted partly linearly to the spinal cord and muscles. Multiple views on the functional relevance of beta activity in the motor system have been proposed. Previous simulation work suggested that pools of spinal motoneurons (MNs) receiving a common beta input could demodulate this activity, transforming it into low-frequency neural drive that could alter force production in muscles. This may suggest that common beta inputs to muscles have a direct role in force modulation. Here we report the experimental average levels and ranges of common beta activity in spinal MNs projecting to single muscles and use a computational model of a MN pool to test if the experimentally observed beta levels in MNs can influence force. When beta was modelled as a continuous activity, the

**Blanka Zicher** obtained her bachelor's and master's degrees in neuroscience from University College London. She is currently doing her PhD at Imperial College London as part of the UKRI Centre for Doctoral Training in AI for Healthcare and in collaboration with Meta. Her PhD research focuses on motor control and neural interfaces.



amplitude needed to produce non-negligible changes in force corresponded to beta representation in the MN pool that was far above the experimental observations. On the other hand, when beta activity was modelled as short-lived events (i.e. bursts of beta activity separated by intervals without beta oscillations), this activity approximated levels that could cause small changes in force with estimated average common beta inputs to the MNs compatible with the experimental observations. Nonetheless, bursting beta is unlikely to be used for force control due to the temporal sparsity of this activity. It is therefore concluded that beta oscillations are unlikely to contribute to the voluntary modulation of force.

(Received 31 May 2022; accepted after revision 30 September 2022; first published online 12 October 2022)

**Corresponding authors** Jaime Ibáñez: BSICoS group, I3A Institute, University of Zaragoza, IIS Aragón, Zaragoza 50009, Spain. Email: jibanez@unizar.es; Dario Farina: Department of Bioengineering, Imperial College, Royal School of Mines, London SW7 2AZ, UK. Email: d.farina@imperial.ac.uk

**Abstract figure legend** This work studied a potential role of beta oscillatory activity (13–30 Hz) on force production. Through simulation of different patterns of beta inputs to a spinal motoneuron pool, we looked at how force production can be affected by this oscillatory activity. The levels of beta, quantified with intramuscular coherence measures, were compared to experimental values. The results suggest that beta oscillatory activity is unlikely to contribute to voluntary force modulation.

### Key points

- It has been previously proposed that beta (13–30 Hz) common inputs to a motor neuron pool may have a non-linear effect in voluntary force control.
- The needed strength of beta oscillations to modulate forces has not been analysed yet.
- Based on computer simulations, we show that sustained beta inputs to a spinal motoneuron pool at physiologically reported levels have minimal effect on force.
- Levels of sustained beta rhythmic activity that can cause a significant change in force are not compatible with experimental observations of intramuscular coherence in human skeletal muscles.

## Introduction

Oscillatory activity in the beta band (13–30 Hz) is prominent in the motor nervous system of primates (Baker, 2007; Baker et al., 1997, 1999; Engel & Fries, 2010; Gilbertson et al. 2005; Kilner et al. 2000; Schoffelen et al. 2005) and, in humans, numerous neurological diseases affecting motor control have been associated with abnormal cortical beta activity (Bichsel et al. 2021; Brown et al. 2001; Hammond et al. 2007; Proudfoot et al. 2018). Beta rhythms have been shown to be transmitted from the brain to the muscles, which makes the study of these signals a particularly relevant tool for assessing cortico-spinal transmission in humans (Baker, 2007; Conway et al. 1995; Baker et al. 1997; Salenius et al. 1997; Zokaei et al. 2021; Engel & Fries, 2010).

Despite its salience, the functional role of beta oscillatory activity is yet unclear. Due to the biomechanical properties of muscles, the inputs that muscle fibres receive at high frequencies (i.e. >10 Hz) have a negligible effect on force production (Farina & Negro, 2015; Farina et al. 2014; Negro & Farina,

2011; Negro et al. 2016). This implies that the linear contributions of beta projections to muscles are irrelevant for motor control. However, previous simulation studies have suggested that MNs may determine non-linear transformations of the high-frequency inputs they receive, converting them into low-frequency activity that could drive muscle contractions (Watanabe & Kohn, 2015). This would be in agreement with recent findings indicating that beta activity can be transmitted with the physiologically shortest delay to muscles, which suggests that using beta to transmit motor commands could provide a way for low latency motor control compared to using non-modulated low frequency signals (Ibáñez et al. 2021). However, critically, the theoretical levels of beta that would be needed to non-linearly affect the neural drive to muscles and therefore force generation are unknown. An alternative view of beta rhythms suggests that this activity may be generated in short-lived bursts at relatively low rates (Zokaei et al. 2021). This would imply that the role of beta in force modulation would not be suitable for continuous control, but it would rather act as an event signal.

The current work studied the association between levels of common beta inputs to MNs and their capacity to modulate forces produced by the innervated muscles. For this purpose, we considered different scenarios of beta activity, ranging from sustained beta oscillations to short-lived bursting beta. Closed-loop simulations by computational models of a MN pool were used to determine the input to the MNs such that a target force was achieved. The effect of adding various levels and dynamics of beta activity to this input was assessed in terms of force change. In addition, the possibility of sustained beta activity being used to directly modulate force was considered. The results from the simulations were compared to experimental data.

## Methods

In this study, we aimed to understand how force production can be affected with different dynamics of beta (continuous to short periods of high amplitude). To address this, we ran a series of simulations of a MN pool to test how various scenarios of common beta inputs to MNs could change force. Reference levels of beta in MN pools were also determined from experimental data. The data, models used, and scenarios considered are described in the next sections.

## Ethical approval

Experimental data were recorded from a total of 28 participants (ages 22–40, 3 females). All subjects gave written informed consent. The study was approved by the University College London Ethics Committee and was conducted in accordance with the *Declaration of Helsinki* (Ethics Application 10037/001), except for registration in a database.

**Muscle recordings.** High-density surface electromyography (HD-sEMG) signals were recorded from the right tibialis anterior (TA), abductor digiti minimi (ADM) and first dorsal interosseous (FDI) muscles at a sampling frequency of 2048 Hz. The electrode grids consisted of 64 electrodes in a  $13 \times 5$  arrangement with an interelectrode distance of 8 mm for the TA and 4 mm for ADM and FDI (OT Bioelettronica, Torino, Italy). Ankle dorsiflexion force was recorded from the TA with the right foot placed under a custom-made lever, knees bent at  $90^\circ$ . To measure force from FDI and ADM, subjects had to place their right hand on a flat surface with the palm facing down. All fingers, except index (for FDI recordings) or little (for ADM recordings) were restrained from moving using a strap. Subjects were instructed to push against a force transducer with their finger (BTP 200; Biometrics Ltd, Newport, UK).

**Task.** At the beginning of the recording sessions, participants were asked to perform maximum voluntary contractions (MVCs) with the studied muscle. To assess beta levels during isometric contractions, subjects were asked to follow a target force consisting of ramp and steady phases. First, force trajectories increased linearly until a target of 5% MVCs (ADM) or 10% MVCs (FDI and TA) was achieved, after which participants were instructed to hold the contraction for 60 s. We selected isometric tasks as beta activity in the brain and muscles is expected to be largest during steady contractions (Engel & Fries, 2010).

## Simulations

**Motoneuron pool.** The MN pool used for the simulations consisted of 25 slow-type MNs, that represented the type of units active during a low-level force output (Henneman 1957; Henneman et al, 1974; Binder et al. 1996). Slow-type MNs were chosen to simulate beta activity during mild contractions (Schoffelen et al. 2005; 2008). Increasing the number of simulated MNs did not substantially influence the results, as assessed in pilot analyses (results not shown).

For all simulations, the MNs received both common inputs (same for all MNs) and independent inputs. The common input always contained a form of beta oscillatory activity. As a simplification, beta rhythms for most simulations were represented as a 20 Hz sinusoidal signal (Watanabe & Kohn, 2015; 2017). Independent inputs were in the form of white Gaussian noise.

Each MN in the simulated pool was represented as a conductance-based two-compartmental model, based on previously published work (Cisi & Kohn, 2008). The structure of each MN consisted of a dendritic and a somatic compartment. The soma contained the leak,  $\text{Na}^+$ , fast  $\text{K}^+$  and slow  $\text{K}^+$  currents, while the dendrite had leak currents besides the synaptic input currents. In this model, all excitatory inputs were combined into one. The resting membrane potential was set to 0 mV and the Nernst equilibrium potentials were adjusted accordingly. For the somatic and dendritic compartments, the membrane potential change over time was described by eqns (1) and (2) (Cisi & Kohn, 2008), respectively:

$$\frac{dV_s(t)}{dt} = -\frac{1}{C_s} \left\{ g_c [V_s(t) - V_d(t)] + g_{Ls} [V_s(t) - E_L] + g_{\text{Na}} m^3 h [V_s(t) - E_{\text{Na}}] + g_{\text{Kf}} n^4 [V_s(t) - E_{\text{K}}] + g_{\text{Ks}} q^2 [V_s(t) - E_{\text{K}}] \right\}, \quad (1)$$

$$\frac{dV_d(t)}{dt} = -\frac{1}{C_d} \left\{ g_c [V_d(t) - V_s(t)] + g_{Ld} [V_d(t) - E_L] + g_e [V_d(t) - E_e] \right\}. \quad (2)$$

In the above equations,  $V_s$  and  $V_d$  represent the somatic and dendritic membrane potentials;  $C_s$  and  $C_d$  the somatic and dendritic membrane capacitances;  $E_{Na}$  and  $E_K$  the sodium and potassium equilibrium potentials;  $g_{Na}$ ,  $g_{Kf}$ ,  $g_{Ks}$  the sodium, fast potassium and slow potassium conductances;  $E_L$  the leak equilibrium potential;  $g_{Ls}$  and  $g_{Ld}$  the leak conductances for soma and dendrite,  $g_c$  the coupling conductance;  $g_e$  and  $E_e$  the conductance and reversal potential for excitatory synapses. The rate constants  $m$ ,  $h$ ,  $n$ ,  $q$  are for sodium activation, inactivation, fast potassium activation and slow potassium activation. A pulse-based model was used for these rate constants (Destexhe, 1997; Cisi & Kohn, 2008). The coupling conductance, membrane capacitances and leak conductances were calculated using eqns (3), (4) and (5) (Cisi & Kohn, 2008):

$$g_c = \frac{2}{\frac{R_i l_d}{\pi r_d^2} + \frac{R_i l_s}{\pi r_s^2}}, \quad (3)$$

$$C_x = 2\pi r_x l_x C_m, \quad (4)$$

$$g_{lx} = \frac{2\pi r_x l_x}{R_{mx}}, \quad (5)$$

where  $R_i$  is cytoplasm resistivity (set to  $70 \Omega \text{ cm}$ );  $r_s$ ,  $r_d$ ,  $l_s$ ,  $l_d$  are somatic and dendritic radius and length;  $x$  denotes the compartment;  $C_m$  is membrane specific

capacitance (set to  $1 \mu\text{F}/\text{cm}^2$ );  $R_{ms}$  and  $R_{md}$  ( $R_{mx}$ ) are somatic and dendritic membrane specific resistances. The differential eqns (1) and (2) were solved with the fourth order Runge-Kutta method.

The twitch response of each motor unit was modelled as a second-order critically damped system with MN spikes represented as Dirac impulses (Cisi & Kohn, 2008). The total force produced was calculated by summing all motor unit responses.

All parameter values used in the S-type MN models were taken from Cisi & Kohn (2008). The models were custom implemented using Julia programming language (<https://julialang.org/>).

**Simulation runs.** To test a potential role of beta oscillatory activity in force modulation, both closed-loop and open-loop simulations were run (Fig. 1). In the closed-loop simulations, a proportional-integral-derivative (PID) control algorithm controlled the common input to the pool in such a way that a target force was tracked (Fig. 1A). In this case, the PID directly modulated the excitatory synaptic conductance (see eqn (2)). In the open-loop simulations, sustained or bursting common beta inputs of various levels were added to a low-frequency common drive to measure how force changed (Fig. 1B).

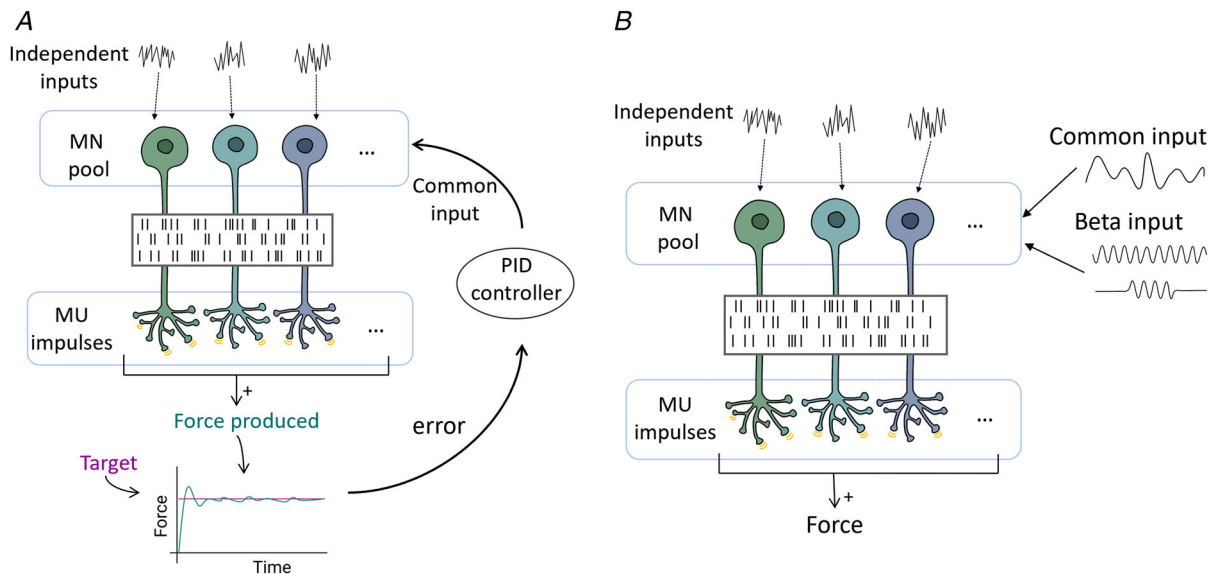


**Figure 1. Schematics of the simulations**

A, in the closed-loop simulations, a PID controller set the common input to the pool such that a target force was achieved. Only three MNs are shown. On each iteration, MN responses to the given inputs were calculated from the two-compartmental models. Total force was then computed as the sum of twitch responses from all motor units. Finally, the error between the target and force produced was fed back to the controller which updates the input. B, in open-loop simulations, the pool received three inputs: independent, low-frequency common drive and a common beta. The low frequency common inputs were previously generated using a closed-loop simulation with an unrestricted controller that had to track a constant force target. Beta inputs were represented as either sustained or concentrated in short-lived bursts.

In the first set of simulations, we tested whether any non-negligible changes in force could be produced when a sustained, constant amplitude beta input was added to a low frequency common drive created by the PID. This common input was set by an unrestricted controller such that a constant force was achieved. The level of beta was determined in such a way that intramuscular coherence values (see details in the Data analysis section) were below 0.6, to reproduce results reported in the experimental part of this study. We report the levels of beta inputs as the percentage that beta amplitude represented out of the total common input: (amplitude of sinusoid/total low frequency common input)  $\times$  100. Three different noise levels were tested to make sure the ratio of independent to common inputs did not affect the reached conclusions. The independent inputs were represented as Gaussian noise with a standard deviations of 0.015 nS, 0.03 nS and 0.045 nS, which is equal to 7%, 15% and 23% of common input.

As in the first simulations beta was a pure 20 Hz sinusoid, we tested whether having beta represented with a larger bandwidth (15–25 Hz) would affect the results. We therefore ran a simulation with the same low-frequency common and independent input parameters as in the case in which independent inputs were 15% of the common inputs (outlined above) but with beta input generated as bandpass filtering (using bandpass function in Matlab) Gaussian noise. The variance of the filtered noise was set so that the resulting IMC peak in beta was 0.6. The effect on force was then compared to the control.

To test whether beta inputs could track different force traces, the frequency content of the common input controlled by the PID was restricted in the next simulation. In this case, the PID controller was setting the amplitude of a predefined 20 Hz sinusoidal input to the MNs, with a step size of 1 ms. The mean level of input (DC component summed to the beta inputs) was chosen in a such a way that a certain force level was reached when the power in beta was 0. The independent inputs were Gaussian noise with standard deviation of 0.015 nS (equal to 7% common input), as in the last simulations. This setup allowed us to test whether force changes can be controlled by modulating the amplitude of beta. We tested two different target force traces. First, a force target with step changes from 5 to 10 N had to be followed by the PID. The mean input was set such that, with no beta, the force produced would be 5 N. Therefore, in order to increase force (reach 10 N), the power of the beta input to MNs had to be modulated as soon as the step change took place. In the next case, smaller, 1 Hz sinusoidal force changes in the target had to be tracked by the controller. Again, the mean input was set such that in all conditions an  $\sim$ 8 N force was produced in the absence of beta inputs. The amplitudes of the 1 Hz targets were chosen so that the forces produced had coefficients of variation

(COV) of 9%, 6% and 3%. The lowest COV tested here matches experimental observations for a condition in which a muscle produces  $\sim$ 10% of the maximum voluntary contraction (MVC) (see Experimental results).

Next, the case of beta transmitted as short-lived events (or bursts) was studied. Again, each MN received a low-frequency common input and independent input in form a Gaussian noise with a standard deviation equal to 23% common input. The amplitude and rate of bursts was varied, while the length of the bursts was fixed to 150 ms (equal to 3 cycles of the 20 Hz sinusoid) (Echeverria-Altuna et al. 2022). The simulations were run 30 times for each of the 10 conditions tested in total: a control with no beta input to the pool, three different levels (amplitudes) of beta, each with three different rates of bursts. For each run, a new beta input was created according to the parameters (rate and amplitude of bursts), to vary the exact time when bursts happened. As the location of the bursts could affect the intramuscular (IMC) values (see Coherence measures in Data analysis), the simulations were run multiple times to get an estimate of the variation between runs. A rate of 0.5 Hz means that the bursts were happening on average every 2 s. Equivalently, at 0.67 Hz and 1 Hz, the average time between bursts was 1.5 s and 1 s, respectively. A 20% variation in when the bursts happened was added to all three cases. The amplitudes were chosen empirically, such that the largest level of beta had a small effect on force.

The previous open-loop simulations mostly assessed extreme cases of beta, with either a continuous, constant amplitude or rectangular bursts of fixed durations. To quantify how force changes were affected by the dynamics of beta inputs, we generated a spectrum of beta oscillatory activity by modulating a 20 Hz sinusoid with a low frequency noise of increasing variances. The modulatory signals were generated by first low-pass filtering (2nd order Butterworth) Gaussian noise with a cut-off frequency of 3 Hz. This value was chosen to simulate the low rate of bursts reported in previous work (Bräcklein et al. 2022; Echeverria-Altuna et al. 2022). To create 15 different cases with increasing variance of the signal, the standardized low-frequency noise was multiplied by a range of values from 0.01 to 1. It was then thresholded at 0.7 to create periods of zero beta amplitude in the later cases, by setting the values below the threshold to zero. The value of the threshold was chosen such that, the time of zero amplitude increased linearly from case 5 onwards, reaching more than 5 s out of the 20 s simulation in case 15 (lowering the threshold had a saturating effect on the time of zero amplitude). In the first four cases, there were no periods of zero amplitude. Finally, beta inputs were created by multiplying the sinusoid with the generated modulatory signals. Open-loop simulations were run with the low-frequency common inputs and Gaussian noise independent inputs set to the same levels

as in the last two cases from the first simulations. Force changes were quantified by comparing the mean force level and COV values to the control case (no beta input).

**Optimisation of controller.** The PID parameters  $K_p$ ,  $K_i$  and  $K_d$  were optimised using particle swarm optimisation (PSO) (Pornsing et al. 2015; Shi & Eberhart, 1999; Tripathi et al. 2007). PSO uses eqn (6) to update particle  $i$ 's velocity at time  $t + 1$  based on the current position ( $x_i$ ), the local best ( $pbest_i$ ) and global best ( $gbest$ ) positions. The new position is then updated using the velocity.

$$v_i^{t+1} = \omega v_i^t + \varphi_1 \beta_1 (pbest_i^t - x_i^t) + \varphi_2 \beta_2 (gbest^t - x_i^t). \quad (6)$$

The inertia ( $\omega$ ), cognitive ( $\varphi_1$ ) and social ( $\varphi_2$ ) weights change over time in such a way that the search focuses more on the local area in the beginning of the optimisation (eqns (7), (8) and (9));  $\beta_1$  and  $\beta_2$  are random numbers between 0 and 1.

$$\omega = 0.9 - \frac{0.9 - 0.4}{T}t, \quad (7)$$

$$\varphi_1 = \frac{0.5 - 2.5}{T}t + 2.5, \quad (8)$$

$$\varphi_2 = \frac{2.5 - 0.5}{T}t + 0.5, \quad (9)$$

with  $t$  representing the current cycle number and  $T$  the total number of cycles. To find the best particle position (PID parameters), the integral of time-weighted absolute error (ITAE) was used, described by eqn (10):

$$ITAE = \int t |e(t)| dt \quad (10)$$

Where  $e(t)$  is the error at time  $t$ .

## Data analysis

**HD-sEMG decomposition.** Experimental data recorded from the muscle was filtered (20–500 Hz, second order zero-lag Butterworth) and decomposed into constituent spike trains with previously validated methods (Holobar et al. 2014; Negro et al. 2016) and the decomposed signals were visually inspected and edited to ensure reliable estimates of motor unit spiking activity (Hug et al. 2021). Only the units active during the interval of interest and those with a pulse-to-noise ratio higher than 30 dB were considered in the analysis.

**Coherence measures.** In coherence measures, only tonically firing units were included. For open loop simulations, MNs activated by the low-frequency input (without beta) were considered (22 out of 25 MNs). In closed-loop simulations, MNs steadily recruited by the

mean level of input (when beta amplitude was 0) were included in the analysis. In the simulations with step target 13 MNs, while in the scenario with sinusoidal target, 20 MNs were firing steadily. To relate the simulation results to physiological values, the IMC was calculated from MN spike trains. This was done by first summing the spike trains from two sub-pools of MNs to get their cumulative spike trains (CST). The power spectral densities of the two CSTs and the cross power spectral density were used to calculate the IMC. The procedure was repeated multiple times with different random sub-pools. This coherence represents a measure of the frequency content of the common input. IMC values were estimated using the Neurospec 2.11 toolbox for Matlab (www.neurospec.org; Mathworks Inc., USA).

When estimating IMC values from experimental data, 40 s of recording was used, with all motor units firing in a stable way. In the simulation results, the first second of each simulation (when force increased from 0 to the target) was discarded in this analysis.

## Results

### Experimental data

In the TA, FDI and ADM muscles,  $19.89 \pm 7.20$ ,  $8.00 \pm 2.86$ , and  $9.36 \pm 2.54$  (mean  $\pm$  standard deviation) motor units were identified and used to calculate coherence values. The average discharge rate across all motor units was  $11.32 \pm 1.87$  pulses/second for ADM,  $12.51 \pm 2.29$  for FDI and  $10.84 \pm 1.69$  for TA muscle. The inter-spike interval coefficient of variation was  $20 \pm 6\%$ ,  $19 \pm 5\%$ ,  $14 \pm 4\%$  for ADM, FDI and TA muscles, respectively. The coefficient of variation of force during the steady part of the contraction was  $4.6 \pm 0.8\%$  for ADM,  $5.5 \pm 0.8\%$  for FDI and  $2.4 \pm 0.8\%$  for TA. Here we report IMC levels measured in the three muscles during isometric contractions. The results are shown in Fig. 2. Average peak IMC values found in beta frequencies (13–30 Hz) were  $0.16 \pm 0.07$  for ADM,  $0.13 \pm 0.07$  for FDI and  $0.29 \pm 0.14$  for TA muscle. Most muscles and subjects led to IMC peaks in beta below 0.5, with only one muscle-subject pair showing a peak above 0.6. The location of the beta peak was variable across subjects, as shown in Fig. 2.

### Sustained beta inputs to MNs at physiological levels have minimal effect on force

In the first simulation, the effect of adding beta oscillations of constant amplitude to the common input to MNs was assessed. The results from three different levels of beta inputs are shown in Fig. 3, with each panel representing simulations with different independent input levels. As

expected, increasing the amplitude of beta resulted in an increase in the IMC at 20 Hz. However, while changing the level of beta inputs strongly affected the obtained levels of intramuscular coherence, it had minimal effect on force, with a very small increase in the mean force level when the largest amplitude beta was compared to the control case (0.79%, 0.42%, and 0.44% increase in the simulations with lowest to highest noise levels, respectively). The average level of force was calculated on the stable part of the force trace. This change in force is unlikely to be behaviourally

relevant, as even if the force produced in the control case is considered to be 100% MVC, the forces were boosted less than 0.8% MVC. Changing the level of the independent inputs to MNs did not change the conclusions.

To test how the bandwidth of the simulated beta input to MNs affected the results, we ran an additional simulation with a wider bandwidth beta input. The model parameters were the same as in the previous simulations, but beta was generated by bandpass filtering white Gaussian noise within 15 to 25 Hz. The variance of this Gaussian noise

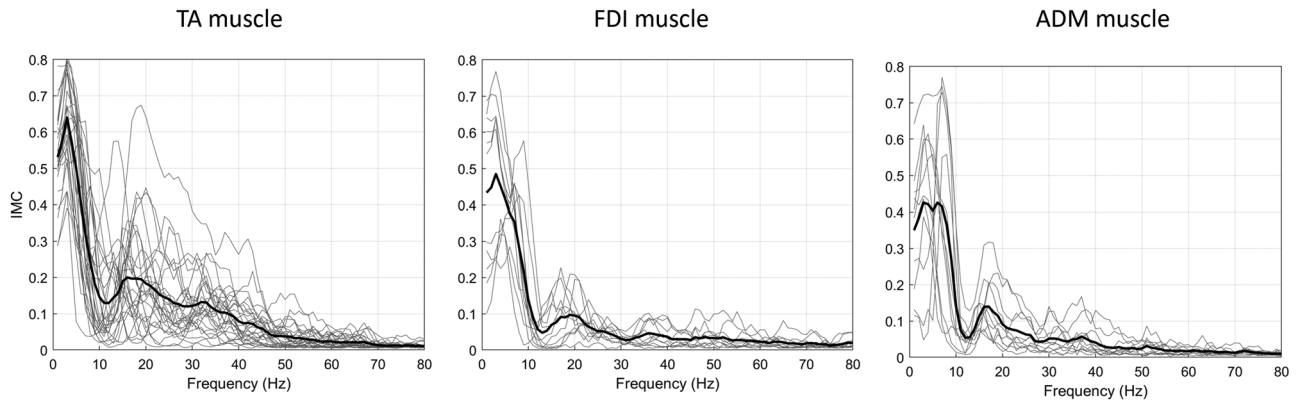


**Figure 2. IMC levels measured experimentally in three different muscles**  
 IMC values for each subject are plotted with grey lines and average values are shown in black. In all three muscles, there are clear peaks at beta frequencies (15–25 Hz). TA muscle data was recorded from 28 subjects, while ADM and FDI muscle data from 11 subjects.

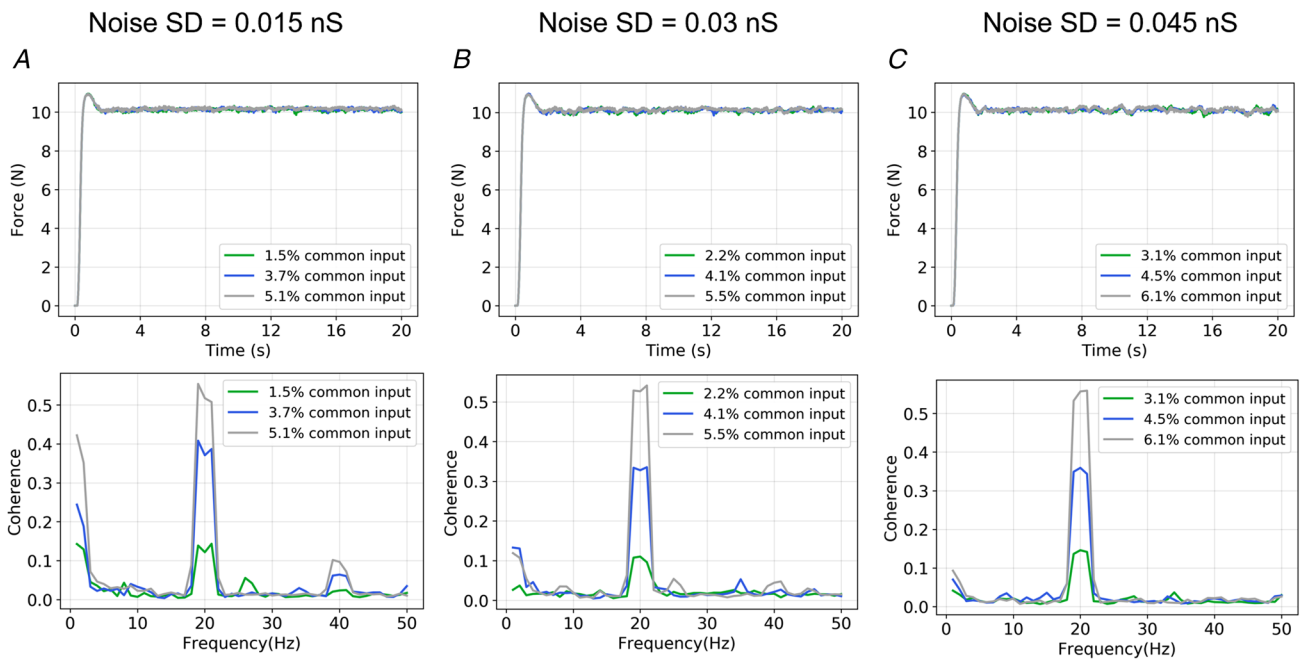


**Figure 3. Increasing beta power with minimal changes in force has a large effect on IMC, regardless of independent input level (reported as unit of electrical conductance)**  
 A, forces produced (upper plot) and intramuscular coherence traces (lower plot) in the simulations with the lowest level of noise. Three different beta amplitude levels were simulated. B, force traces and intramuscular coherence plots with middle level noise. C, force produced and intramuscular coherence results with the highest level of noise tested.

was set such that the resulting IMC peak in beta frequency reached 0.6. The effect on force was minimal, with the mean force level increasing 1.1% compared to the control.

### Beta levels that can modulate force are above physiological values

To study whether force changes can be controlled with power in beta, the common input to the MN pool was restricted to a 20 Hz sinusoid. A PID controller was set to optimally determine beta levels to track various force traces (step and sinusoidal).

In the first scenario, the target force trace had step changes between 5 and 10 N. Figure 4A and B show the results from this simulation. The controller successfully tracked changes in the force target by increasing the amplitude of the 20 Hz sinusoid. The intramuscular coherence, calculated from the spike trains of active MUs over the whole epoch, showed a peak at 20 Hz and its harmonics that saturated to 1, which contrasts with observations from experimental data.

To check how IMC values change when beta is only producing small changes in force, in the second simulation the PID had to reliably track 1 Hz oscillatory targets of different amplitudes. Figure 4C and D shows the force traces and corresponding IMC plots for the three cases which correspond to rhythmic force changes equivalent to 3%, 6% and 9% coefficient of variation. The lowest value was chosen to match the physiological variation at a low-level isometric contraction. The peak coherence values around 20 Hz in these scenarios were 0.91, 0.85 and 0.84, well above the experimental observations. As in the previous tests, we observed here clear peaks at 40 Hz (harmonic of 20 Hz), something not seen experimentally. These harmonics are due to exacerbated beta levels that synchronise MN firings.

### Short-lived beta events may have an effect on force

In the next simulation, the effect on force of various levels of bursting beta was assessed. In these runs, beta was represented by rectangular bursts of three cycles

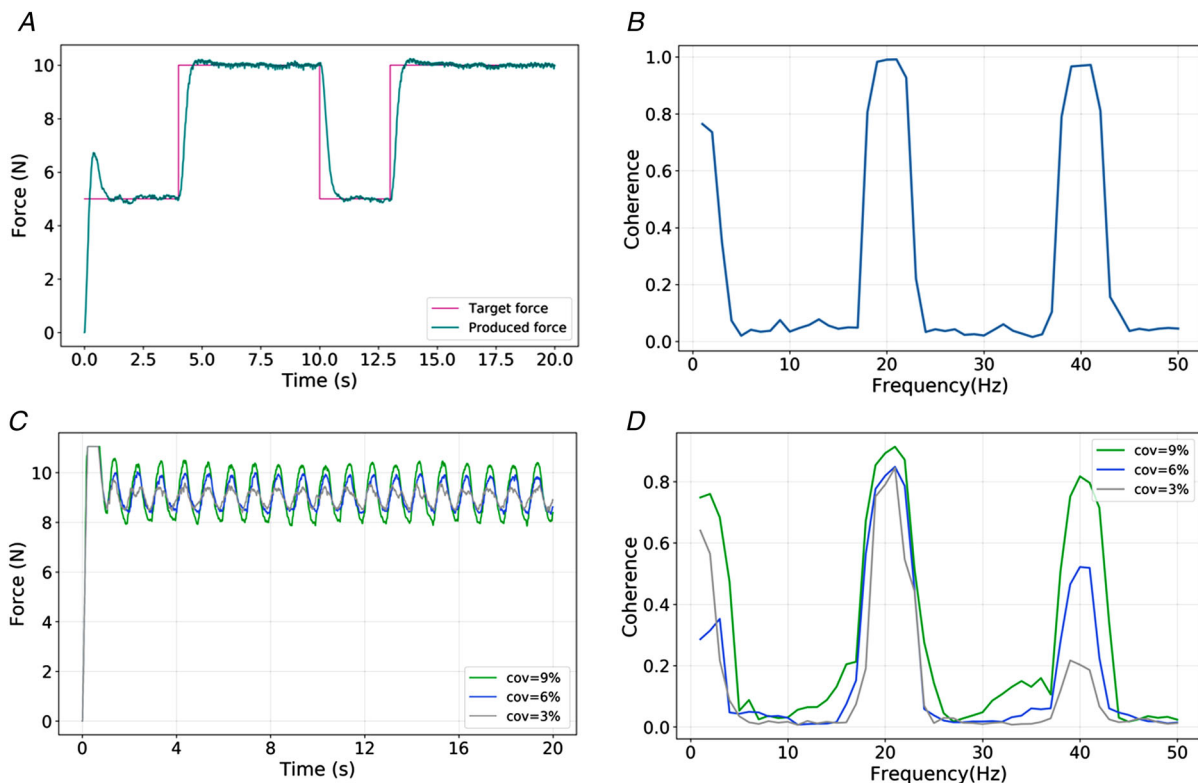


**Figure 4. Force can be controlled by modulating the power in the beta band of the common inputs to MNs**

A, force produced by the motor units (green) and target force tracked (magenta). The target force was made up of step changes between 5 and 10 N. B, intramuscular coherence plot calculated from the spike trains of motoneurons, corresponding to the scenario in A. C, forces produced with different levels of variation. The 20 Hz sinusoid input offset, together with the independent inputs, produces an ~8 N constant force. The target forces were oscillating at 1 Hz. D, intramuscular coherence plots for the three cases described before.



of a 20 Hz sinusoid. As in the first simulations, the unrestricted PID controller was used to directly change conductance to create a common input that resulted in a 10-N constant force. Beta bursting activity was then added as an additional common input to the pool.

In total, nine conditions were tested: three different amplitudes and three different rates of bursts. For each of these, 30 data points were generated. IMC values around 20 Hz increased with increasing rate and amplitude of bursts (Fig. 5A). Panels B, C and D in Fig. 5 show force traces from simulations with bursts happening on average every 1.5 s, with increasing amplitudes. For the largest beta levels (Fig. 5D), transient perturbations in force could be seen compared to when the input contained lower levels of beta (Fig. 5B). These perturbations were observed while IMC levels within the beta band were still within physiological realistic ranges as compared to experimental results.

### Effect on force increases with the amplitude modulation of beta

To study how the variability in beta amplitudes could affect our results, we simulated a set of different beta inputs ranging from constant amplitude signals to beta activity only occurring in the form of bursts with a certain rate and quantified the effects on force for the different types of inputs simulated. To do this, a 20 Hz sinusoid was modulated by a low-frequency noise of different variances. As the variance of the noise increased, the beta input became more burst-like, with the time periods of zero beta amplitude increasing. Figure 6A shows the first case, closest to a constant amplitude beta, while Fig. 6B shows the last case, in which bursts of high amplitude beta can be seen. In these simulations, a total of 15 cases of beta inputs were created, with the low frequency common and Gaussian noise independent inputs kept the same as in Fig. 3B and C.

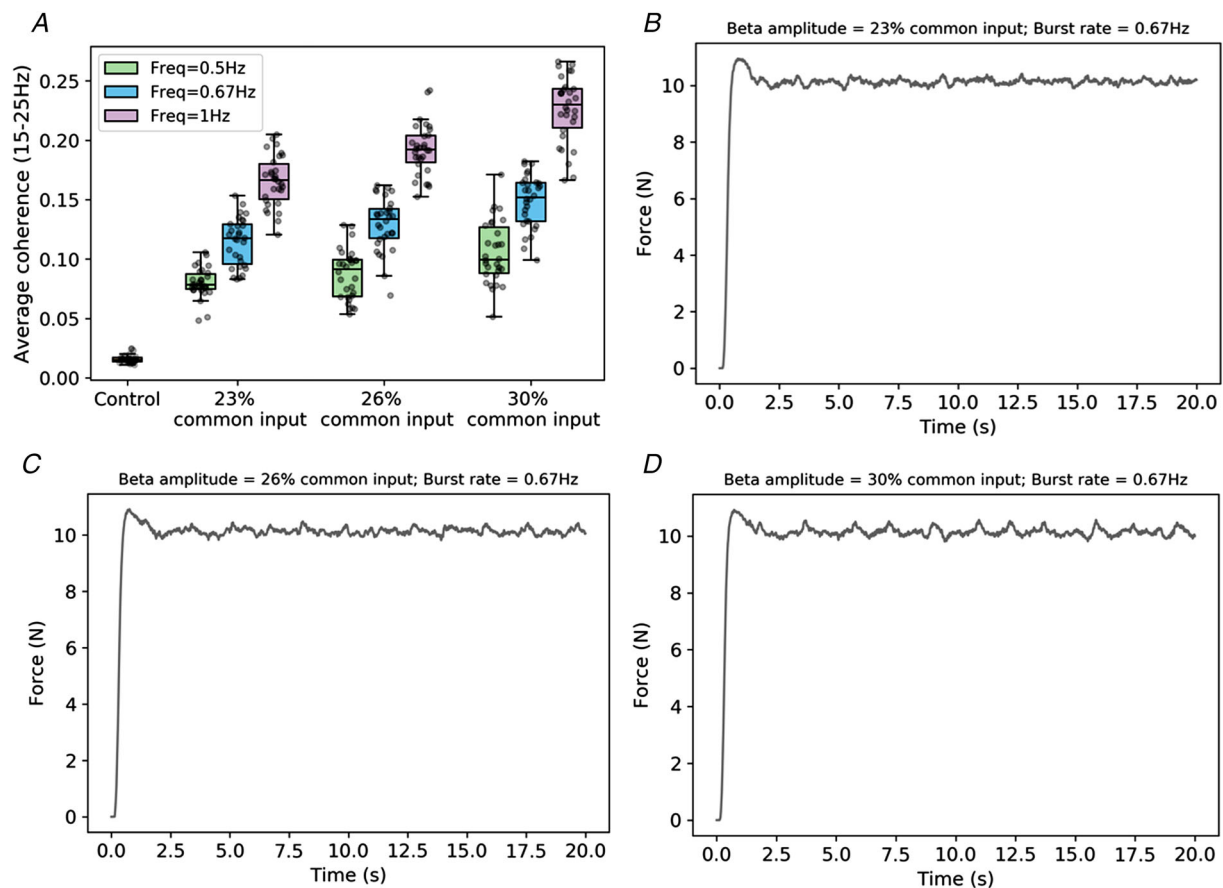


**Figure 5. Intramuscular coherence in the beta band increases with the amplitude and frequency of the bursts**

A, boxplot of average coherence values ( $N = 30$ ) in beta band (15–25 Hz) for 10 different conditions: control with no beta input, three levels of beta with three different burst rates. Beta levels are reported in terms of percentage of the average input level. Individual data shown as grey dots, plotted with jitter for clarity. B, force produced with lowest amplitude of beta with a rate of bursts of 0.67 Hz (every 1.5 s). C, force produced with beta amplitude equal to 26% of common input. Rate of bursts set to 0.67 Hz. D, force produced with largest amplitude of beta simulated (30% common input). Rate of bursts equal to 0.67 Hz.

For the scenario with the first common and independent input parameters, the results show a maximum change in mean force levels of 0.85 (% increase from control level) and a 0.25% increase in the COV of force (Fig. 6C). In the case with larger level of independent inputs, the change in mean force levels was below 0.75%, while the maximum change in COV of force was 0.32% (Fig. 6D). In both cases, the observed changes in force increase with the modulation of beta, but they are minimal compared to the physiologically recorded COV of force reported in the experimental part of this study.

## Discussion

Previous work has suggested a potential role for beta rhythms in force modulation. However, the magnitude of beta levels required to affect force has not been studied. To address this, the current study investigated a potential effect of beta band oscillatory activity on force production using physiologically realistic models and direct comparison with experimental observations. The level of beta common inputs used in the simulations was compared to experimental data from relatively large pools of subjects. Multiple scenarios were tested: from beta represented as sustained rhythms to short-lived events.

The work was based on the assumption that values of coherence outside those reported experimentally cannot reflect real experimental conditions.

In the first part of this work, open-loop simulations were run with beta represented as a continuous signal. The results from the simulations showed that changes in beta amplitudes that increased IMC values from 0.1 to 0.5 (representing the experimental range) resulted in negligible changes in the force traces. To test whether beta can be used directly to modulate force, closed-loop simulations were set up. The controller could successfully adjust power in beta such that step and sinusoidal force traces were tracked. However, even when the changes in force were at 3% COV of force, which is comparable to the variation reported in our experimental results, the level of beta was considerably higher than what could be measured experimentally. Overall, this suggests that sustained beta activity has minimal involvement in force production, contrary to previous suggestions (Watanabe & Kohn, 2015).

We also assessed the situation where beta is a not a continuous signal. There is increasing evidence that at a single trial level, in isometric contractions tasks, the oscillatory activity is transmitted in bursts, instead of as a sustained rhythm (Echeverria-Altuna et al. 2022; Little

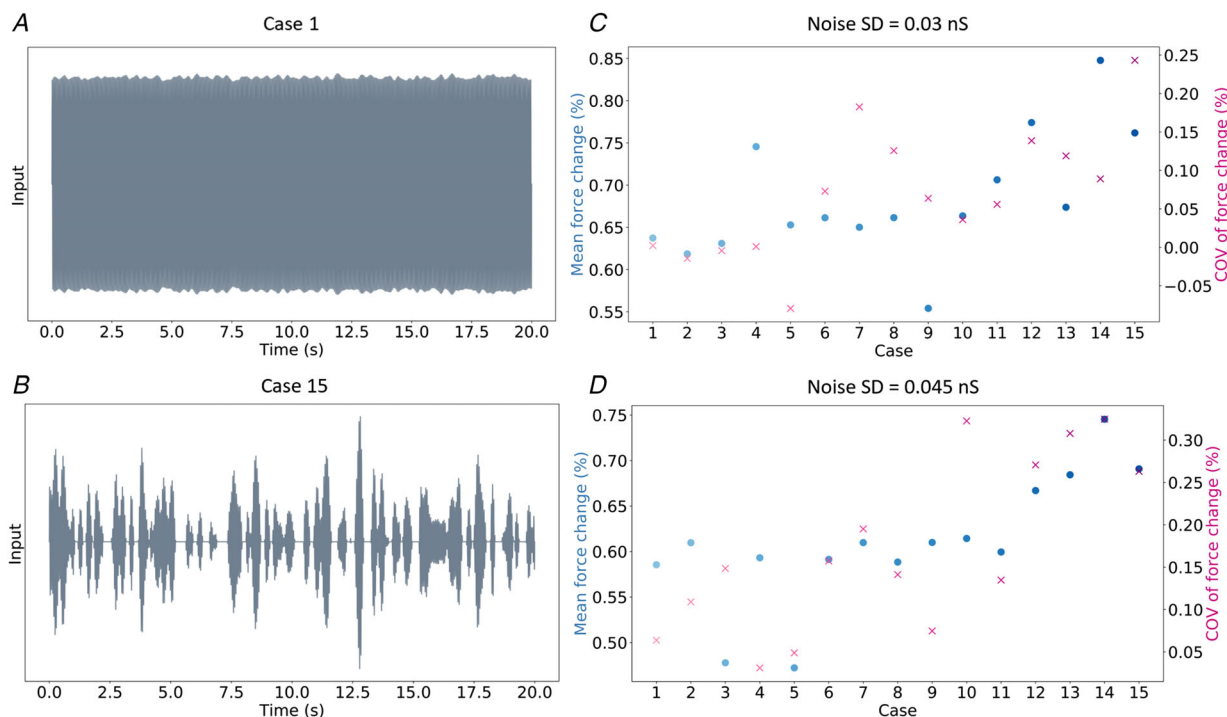


**Figure 6. Mean force and COV increases with beta amplitude modulation**

A, beta input that was simulated as case 1. B, beta input simulated as the last case. C, beta input effect on force in 15 cases tested, with independent noise standard deviation equal to 15% common input. Mean force change (% control) is plotted as filled circles in blue and the change in COV of force is plotted with an  $\times$  in magenta. Beta inputs ranged from continuous (lighter colours) to burst-like (darker colours). D, force changes in the simulations with the noise standard deviation equal to 23% common input. Mean force changes are in blue, while COV changes in magenta.

et al. 2019; Wessel, 2020; Bräcklein et al, 2022). Here, open-loop simulations were run with a common beta input represented as short-lived bursting activity to assess changes in force. Results suggest that, in this case and depending on the actual characteristics of beta bursts (in terms of their rate and amplitudes), it may be possible that beta has an effect on force while still maintaining beta IMC in the MNs at experimentally observed levels. This non-linear effect on forces should be expected to be relatively small according to our results: the required levels of the beta bursts affecting forces resulted in IMC values in the range of 0.8–1, which are much higher than the beta IMC levels seen experimentally (averaging 0.1–0.2 depending on the muscles recorded). Such influence of beta inputs to MNs on force would not be compatible with voluntary control of force due to the temporal sparsity and regularity of the bursting beta.

To understand how the variability of the beta envelope affects forces when values of IMC are fixed, we used different beta inputs ranging from continuous beta (with constant instantaneous amplitude) to beta inputs in the form of short-lived events spaced by periods of no beta. In all these cases, beta power was adjusted to get IMC values of 0.6, which is larger than what is mostly seen experimentally. Our results have shown that as beta is transmitted in shorter bursts of high amplitude, the effect on force, in terms of mean value and COV, increases. Nevertheless, the amplitude of the changes remains small compared to the physiological variation of force output in an isometric contraction.

The results of this study exclude a main direct role of beta transmission to MNs for force control. An alternative hypothesis for beta being indirectly used for force control is a potential role in transmitting state-related information (Baker, 2007; Witham et al. 2011). The idea that ascending pathways contribute to corticomuscular coherence suggests that beta oscillations may play a role in motor control through sensory feedback (Witham et al. 2011). Our results, suggesting that beta is unlikely to have a direct role in force control, are consistent with this view.

Overall, the results are relevant when considering beta activity as a control signal in biofeedback or closed-loop stimulation applications (Bouthour et al. 2019; Fukuma et al. 2018; He et al. 2019; Little et al., 2013, 2016; Rosa et al. 2015). As beta is transmitted from the brain to muscles, extracting beta signals from the muscle recordings, instead of direct brain recordings, could be a promising approach in these systems. The results here are suggestive of how IMC values change with different dynamics of beta.

### Limitations

The computational model used in this study is obviously a large simplification of the neuromuscular system and

therefore the results should be interpreted carefully. Several limitations have to be considered in this regard. First, the two-compartmental model used in this work is one of many structures that have been used in modelling single neurons (Herz et al., 2006). Even if the model used has been extensively validated, the sensitivity of the outcomes to changes in model structure, complexity and parameter values has not been tested. Furthermore, the size of the simulated MN pool is smaller than the expected number of active MNs during voluntary contractions. The relatively small pool size was determined based on the high computational demands of the closed-loop simulations we ran. Nonetheless, in preliminary work to define the final simulation set, we ran additional open-loop simulations with increasing number of MNs and we did not observe any deviations from the conclusions reached with a smaller pool (these results are not shown). Moreover, in our experiments we only simulated MNs corresponding to low fatiguing motor units. As a consequence, our results may not be generalizable to conditions involving high contraction levels. Nonetheless, we cannot identify mechanisms in MN control sufficiently different between lower- and higher-thresholds MNs to expect substantially different results. Regarding the inputs to MNs simulated, the levels of beta simulated in the different tests ran here can only be interpreted in relative terms. To link our simulations to physiological data, we adjusted our model parameters by fixing either beta IMC levels or force changes and checked how the other parameters in the model changed. The proportional level of independent inputs relative to common beta inputs is unlikely to change the main conclusions in this case, as suggested in the Results where multiple noise levels were considered. As the independent input level increased, the beta input (relative to the low frequencies) needed to reach the same IMC values also increased, while the effect on force was similar (shown in Fig. 3). This is expected since the level of coherence at the beta frequency depends on the beta power relative to the independent input. Nevertheless, future work should test how beta inputs change with a linear increase in independent inputs, while keeping IMC levels constant. Finally, in most simulations, beta activity was represented as a pure 20 Hz sinusoid, which is a simplification of the oscillatory signals found in the nervous system. Nonetheless, we also ran an open-loop simulation with a wider bandwidth beta signal, and this suggested similar conclusions as the case of pure beta input.

### References

- Baker, S. N. (2007). Oscillatory interactions between sensorimotor cortex and the periphery. *Current Opinion in Neurobiology*, 17(6), 649–655.

- Baker, S. N., Kilner, J. M., Pinches, E. M., & Lemon, R. N.(1999). The role of synchrony and oscillations in the motor output. *Experimental Brain Research*, **128**(1–2), 109–117.
- Baker, S. N., Olivier, E., & Lemon, R. N.(1997). Coherent oscillations in monkey motor cortex and hand muscle EMG show task-dependent modulation. *Journal of Physiology*, **501**(1), 225–241.
- Bichsel, O., Stieglitz, L. H., Oertel, M. F., Baumann, C. R., Gassert, R., & Imbach, L. L.(2021). Deep brain electrical neurofeedback allows Parkinson patients to control pathological oscillations and quicken movements. *Scientific Reports*, **11**(1), 1–10.
- Binder, M. D., Heckman, C. J., & Powers, R. K.(1996). The physiological control of motoneuron activity. *Comprehensive Physiology*.
- Bouthour, W., Mégevand, P., Donoghue, J., Lüscher, C., Birbaumer, N., & Krack, P.(2019). Biomarkers for closed-loop deep brain stimulation in Parkinson disease and beyond. *Nature Reviews Neurology*, **15**(6), 343–352.
- Bräcklein, M., Barsakcioglu, D. Y., Vecchio, A. D., Ibáñez, J., & Farina, D.(2022). Reading and modulating cortical beta bursts from motor unit spiking activity. *Journal of Neuroscience*, **42**(17), 3611–3621.
- Brown, P., Marsden, J., Defebvre, L., Cassim, F., Mazzone, P., Oliviero, A., Altibrandi, M. G., Lazzaro, V. D., Limousin-Dowsey, P., Fraix, V., Odin, P., & Pollak, P.(2001). Intermuscular coherence in Parkinson's disease: Relationship to bradykinesia. *Neuroreport*, **12**(11), 2577–2581.
- Cisi, R. R., & Kohn, A. F.(2008). Simulation system of spinal cord motor nuclei and associated nerves and muscles, in a web-based architecture. *Journal of Computational Neuroscience*, **25**(3), 520–542.
- Conway, B. A., Halliday, D. M., Farmer, S. F., Shahani, U., Maas, P., Weir, A. I., & Rosenberg, J. R.(1995). Synchronization between motor cortex and spinal motoneuronal pool during the performance of a maintained motor task in man. *The Journal of Physiology*, **489**(3), 917–924.
- Destexhe, A.(1997). Conductance-based integrate-and-fire models. *Neural Computation*, **9**(3), 503–514.
- Echeverria-Altuna, I., Quinn, A. J., Zokaei, N., Woolrich, M. W., Nobre, A. C., & van Ede, F.(2022). Transient beta activity and cortico-muscular connectivity during sustained motor behaviour. *Progress in Neurobiology*, **214**, 102281.
- Engel, A. K., & Fries, P.(2010). Beta-band oscillations-signalling the status quo? *Current Opinion in Neurobiology*, **20**(2), 156–165.
- Farina, D., & Negro, F.(2015). Common synaptic input to motor neurons, motor unit synchronization, and force control. *Exercise and Sport Sciences Reviews*, **43**(1), 23–33.
- Farina, D., Negro, F., & Dideriksen, J. L.(2014). The effective neural drive to muscles is the common synaptic input to motor neurons. *Journal of Physiology*, **592**(16), 3427–3441.
- Fukuma, R., Yanagisawa, T., Tanaka, M., Yoshida, F., Hosomi, K., Oshino, S., Tani, N., & Kishima, H.(2018). Real-time neurofeedback to modulate  $\beta$ -band power in the subthalamic nucleus in pParkinsons disease patients. *eNeuro*, **5**(6), 1–8.
- Gilbertson, T., Lalo, E., Doyle, L., Lazzaro, V. D., Cioni, B., & Brown, P.(2005). Existing motor state is favored at the expense of new movement during 13–35 Hz oscillatory synchrony in the human corticospinal system. *Journal of Neuroscience*, **25**(34), 7771–7779.
- Hammond, C., Bergman, H., & Brown, P.(2007). Pathological synchronization in Parkinson's disease: Networks, models and treatments. *Trends in Neurosciences*, **30**(7), 357–364.
- He, S., Syed, E., Torrecillos, F., Tinkhauser, G., Fischer, P., Pogosyan, A., Pereira, E., Ashkan, K., Hasegawa, H., Brown, P., & Tan, H.(2019). Beta oscillation-targeted neurofeedback training based on subthalamic LFPS in parkinsonian patients. International IEEE/EMBS Conference on Neural Engineering, NER, March:81–84.
- Henneman, E.(1957). Relation between size of neurons and their susceptibility to discharge. *Science (New York, NY)*, **126**(3287), 1345–1347.
- Henneman, E., Clamann, H. P., Gillies, J. D., & Skinner, R. D.(1974). Rank order of motoneurons within a pool: Law of combination. *Journal of Neurophysiology*, **37**(6), 1338–1349.
- Herz, A. V., Gollisch, T., Machens, C. K., & Jaeger, D.(2006). Modeling single-neuron dynamics and computations: A balance of detail and abstraction. *Science*, **314**(5796), 80–85.
- Holobar, A., Minetto, M. A., & Farina, D.(2014). Accurate identification of motor unit discharge patterns from high-density surface EMG and validation with a novel signal-based performance metric. *Journal of Neural Engineering*, **11**(1), 016008.
- Hug, F., Avrillon, S., Vecchio, A. D., Casolo, A., Ibanez, J., Nuccio, S., Rossato, J., Holobar, A., & Farina, D.(2021). Analysis of motor unit spike trains estimated from high-density surface electromyography is highly reliable across operators. *Journal of Electromyography and Kinesiology*, **58**, 102548.
- Ibáñez, J., Vecchio, A. D., Rothwell, J. C., Baker, S. N., & Farina, D.(2021). Only the fastest corticospinal fibers contribute to  $\beta$  corticomuscular coherence. *Journal of Neuroscience*, **41**(22), 4867–4879.
- Kilner, J. M., Baker, S. N., Salenius, S., Hari, R., & Lemon, R. N.(2000). Human cortical muscle coherence is directly related to specific motor parameters. *Journal of Neuroscience*, **20**(23), 8838–8845.
- Little, S., Beudel, M., Zrinzo, L., Foltynie, T., Limousin, P., Hariz, M., Neal, S., Cheeran, B., Cagnan, H., Gratwicke, J., Aziz, T. Z., Pogosyan, A., & Brown, P.(2016). Bilateral adaptive deep brain stimulation is effective in Parkinson's disease. *Journal of Neurology, Neurosurgery, and Psychiatry*, **87**(7), 717.
- Little, S., Bonaiuto, J., Barnes, G., & Bestmann, S.(2019). Human motor cortical beta bursts relate to movement planning and response errors. *PLoS Biology*, **17**(10), e3000479.
- Little, S., Pogosyan, A., Neal, S., Zavala, B., Zrinzo, L., Hariz, M., Foltynie, T., Limousin, P., Ashkan, K., FitzGerald, J., Green, A. L., Aziz, T. Z., & Brown, P.(2013). Adaptive deep brain stimulation in advanced Parkinson disease. *Annals of Neurology*, **74**(3), 449.

- Negro, F., & Farina, D.(2011). Linear transmission of cortical oscillations to the neural drive to muscles is mediated by common projections to populations of motoneurons in humans. *Journal of Physiology*, **589**(3), 629–637.
- Negro, F., Muceli, S., Castronovo, A. M., Holobar, A., & Farina, D.(2016). Multi-channel intramuscular and surface EMG decomposition by convolutive blind source separation. *Journal of Neural Engineering*, **13**(2), 026027.
- Pornsing, C., Sodhi, M. S., & Lamond, B. F.(2015). Novel self-adaptive particle swarm optimization methods. *Soft Computing*, **20**(9), 3579–3593.
- Proudfoot, M., van Ede, F., Quinn, A., Colclough, G. L., Wu, J., Talbot, K., Benatar, M., Woolrich, M. W., Nobre, A. C., & Turner, M. R.(2018). Impaired corticomuscular and interhemispheric cortical beta oscillation coupling in amyotrophic lateral sclerosis. *Clinical Neurophysiology*, **129**(7), 1479–1489.
- Rosa, M., Arlotti, M., Ardolino, G., Cogiamanian, F., Marceglia, S., Fonzo, A. D., Cortese, F., Rampini, P. M., & Priori, A.(2015). Adaptive deep brain stimulation in a freely moving parkinsonian patient. *Movement Disorders*, **30**(7), 1003.
- Salenius, S., Portin, K., Kajola, M., Salmelin, R., & Hari, R.(1997). Cortical control of human motoneuron firing during isometric contraction. *Journal of Neurophysiology*, **77**(6), 3401–3405.
- Schoffelen, J. M., Oostenveld, R., & Fries, P.(2005). Neuronal coherence as a mechanism of effective corticospinal interaction. *Science*, **308**(5718), 111–113.
- Schoffelen, J. M., Oostenveld, R., & Fries, P.(2008). Imaging the human motor system's beta-band synchronization during isometric contraction. *Neuroimage*, **41**(2), 437–447.
- Shi, Y., & Eberhart, R. C.(1999). Empirical study of particle swarm optimization. *Proceedings of the 1999 Congress on Evolutionary Computation, CEC*, **3**, 1945–1950.
- Tripathi, P. K., Bandyopadhyay, S., & Pal, S. K.(2007). Multi-objective particle swarm optimization with time variant inertia and acceleration coefficients. *Information Sciences*, **177**(22), 5033–5049.
- Watanabe, R. N., & Kohn, A. F.(2015). Fast oscillatory commands from the motor cortex can be decoded by the spinal cord for force control. *Journal of Neuroscience*, **35**, 13687–13697.
- Watanabe, R. N., & Kohn, A. F.(2017). Nonlinear frequency-domain analysis of the transformation of cortical inputs by a motoneuron pool-muscle complex. *IEEE Transactions on Neural Systems and Rehabilitation Engineering*, **25**, 1930–1939.
- Wessel, J. R.(2020).  $\beta$ -bursts reveal the trial-to-trial dynamics of movement initiation and cancellation. *Journal of Neuroscience*, **40**, 411–423.
- Witham, C. L., Riddle, C. N., Baker, M. R., & Baker, S. N.(2011). Contributions of descending and ascending pathways to corticomuscular coherence in humans. *The Journal of Physiology*, **589**, 3789–3800.
- Zokaei, N., Quinn, A. J., Hu, M. T., Husain, M., van Ede, F., & Nobre, A. C.(2021). Reduced cortico-muscular beta coupling in Parkinson's disease predicts motor impairment. *Brain communications*, **3**(3), fcab179.

## Additional information

### Data availability statement

Individual datapoints ( $n \leq 30$ ) are included in the figures. Data from the study will be made available upon reasonable request.

### Competing interests

None.

### Author contributions

B.Z.: conceptualization, investigation, analysis, writing – review and editing; J.I.: conceptualization, investigation, writing – review and editing; D.F.: conceptualization, resources, writing – review and editing. All authors have approved the final version of the manuscript and agree to be accountable for all aspects of the work. All persons designated as authors qualify for authorship, and all those who qualify for authorship are listed.

### Funding

This study was supported by the European Commission grant H2020 NIMA (FETOPEN 899626). B.Z. was supported by the UKRI CDT in AI for Healthcare (Grant No. EP/S023283/1) and by a studentship funded by Reality Labs at Meta; J.I. received the support from 'la Caixa' Foundation (ID 100010434; fellowship code LCF/BQ/PI21/11830018).

### Acknowledgements

The authors are grateful to Dr Daniel Wetmore for insightful comments to the manuscript that helped improve its quality and to Olaoluwa Ayeko for contributions to parts of the simulation code that was used in this work.

### Keywords

beta rhythms, coherence, motor control, motor units

## Supporting information

Additional supporting information can be found online in the Supporting Information section at the end of the HTML view of the article. Supporting information files available:

### Statistical Summary Document

### Peer Review History

### Data set for TA muscle

### Data set for FDI muscle

### Data set for ADM muscle